Zinc Positioning's Impact on Electrochemical Stability of γ-Al_2O_3 for Supercapacitor Efficiency

Deepannita Chakraborty[1,*], S. Maruthamuthu[1], Tholkappiyan Ramachandran[1,2], N. Priyadharsini[3], S. Kaleemulla[4]

[1]*Department of Physics, PSG Institute of Technology and Applied Research, Coimbatore, 641 062, India.*
[2]*Department of Physics, Khalifa University of Science and Technology, Abu Dhabi, P. O. Box 127788, United Arab Emirates.*
[3]*Department of Physics, Dr. N. G .P. Institute of Technology, Coimbatore, 641 048, India*
[4]*Thin Film Laboratory, Centre for Functional Materials, Vellore Institute of Technology, Vellore, 632 014, India*

Corresponding Author: monkaichakraborty@gmail.com

Abstract

The electrochemical properties exhibited by the zinc-doped alumina nanoparticles suggest their potential as another viable alternative for supercapacitor electrode applications. The strategic placement of Zn^{2+} ions within the interstices of the alumina lattice forms potential barriers between Al^{3+} and Zn^{2+} ions, acting as effective centers for trapping charges. The structural changes reports decrease in the average crystallite size from 9 nm to 5 nm. The formation of trapping centers is confirmed by the enhancement in optical band gap value from 1.89 eV to 4.21 eV. The XPS data confirms the oxidation state of +3 and +2 for Al and Zn ions, respectively. A prolonged charge retention and an increased energy storage density, is evidenced by the observed value of 1237 F g^{-1} at 1 A g^{-1}. Furthermore, the stability of alumina gets enhanced on doping, demonstrating for the first time an impressive 92% stability over 10000 cycles. The 5% Zn-doped Al_2O_3 electrode has the highest diffusion coefficient of 8.9×10^{-12} cm^2 s^{-1}, showing efficient active sites for electrolyte ion intercalation. The asymmetric supercapacitor device analysis with 5% Zn doped alumina as one of the electrodes attains a stability of 85% after 5000 repeated cycles. The device achieves better energy density value of 47.63 W h kg^{-1} at a power delivery rate of 996.9 W kg^{-1} .This study offers valuable insights into the electrochemical performance of zinc-doped alumina nanoparticles, underscoring their potential for high-performance energy storage applications in supercapacitors devices.

Keywords: Intercalation Pseudocapacitance; specific capacitance; γ-Al_2O_3; electrochemical stability; supercapacitors.

1 Introduction

The drive to create nanoscale energy storage solutions has spurred investigations into a novel category of materials known as Supercpacitors (SCs). These cutting-edge materials have demonstrated exceptional efficiency in both the storage and extraction of energy [1]. SCs heralded as versatile energy reservoirs, have found utility not only within the Internet of Things

domain [2-4], but also within the critical sphere of healthcare services [5-7]. Researchers have delved into an array of oxides and sulfides in their quest to fashion these materials into SCs [8-16]. Yet, a significant hurdle persists in the quest for efficient SCs [17-19]. The energy-harnessing abilities of SCs are intricately intertwined with an assortment of parameters, including porosity, pore volume, and interlayer distance[20]. These factors serve as pivotal determinants in the efficiency with which these devices store charges. SCs operate on multiple mechanisms, each possessing their own distinctive method of storing energy. These mechanisms encompass: 1. Electrochemical Double Layer 2. Pseudocapacitance 3. Hybrid Capacitance. An intricate grasp of these phenomena and their optimization are pivotal to advancing the efficacy of SCs as efficient energy reservoirs. As ongoing research continues to explore novel materials and design strategies, the potential for SCs to redefine energy storage across diverse industries remains compelling.

Among these mechanisms, Pseudocapacitors stand out for their dual approach to charge transfer, utilizing both chemical and electrostatic means. Materials exhibiting pseudocapacitance have demonstrated remarkable energy storage density, effectively surmounting the challenges encountered by traditional batteries and electrode double layer cells [21]. Pseudocapacitance emerges within semiconductors because of various defects or through intercalative arrangements. The intercalative structure signifies the presence of impurities nestled within the host lattice's interstitial spaces. In conjunction with this intercalative arrangement, the porous nature of semiconductors further amplifies pseudocapacitance. These pores serve as potential barriers, adept at capturing charges and releasing them upon reaching a specified potential in opposing directions. The degree of porosity within the SC material directly correlates with its energy storage density [22, 23]. This intricate interplay of structure and chemistry underscores the potential of pseudocapacitive materials to drive advancements in energy storage technologies[24, 25].

In this study, gamma alumina (γ-Al_2O_3) is used as the host material with zinc oxide (ZnO) as the dopant. Zinc oxide offers efficient vacant sites for electrochemical properties [26], while alumina is known for its solar and thermal energy storage capacities [27-29]. The study focuses on how the arrangement of zinc ions within the host lattice enhances electrochemical stability and specific capacitance of alumina nanoparticles. This work advances energy storage materials by focusing on (i) long term stability and durability, (ii) enhanced specific capacitance (iii) detailed insight on the mechanics behind intercalative pseudocapacitance, clarifying the interplay between zinc and aluminium ions. It also highlights the importance of optimizing dopant concentration to achieve the best electrochemical performance. It presents a promising path for high-performance SCs, potentially surpassing traditional lithium-ion batteries in stability and efficiency for sustainable energy solutions. Beyond SCs, the findings could have broader implications for other energy storage systems, such as batteries and hybrid capacitors, where high capacity, stability, and fast charge-discharge capabilities are required. The innovative approach of using Zn-doping to enhance the properties of Al_2O_3 contributes to the broader field of material science, offering a new pathway to engineer materials with superior performance characteristics. Overall, this research work advances the understanding and application of Zn-doped Al_2O_3 in energy storage technologies, paving the way for the

development of more efficient, stable, and high-performing SCs. The chosen material exhibited properties suitable for making highly sustainable and stable asymmetric SC device.

2 Experimental Method

The oxide precursors of zinc (ZnO, Sigma Aldrich (Merck), 99.99% purity, nanopowder) was acquired from Merck, ensuring a reliable starting point for the synthesis process. The pure alumina nanoparticles were meticulously prepared by grinding aluminum hydroxide ($Al(OH)_3$, Sigma Aldrich (Merck), 99.99% purity, nanopowder) powder for 8 hours using agate mortar and pestle, followed by sintering at 900 °C for 4 hours in a muffle furnace. This precise method ensures the formation of high-quality alumina nanoparticles with the desired properties. To create the zinc-doped alumina ($Zn:Al_2O_3$) samples, the stoichiometric combination of zinc and aluminum was calculated for various doping concentrations. The resulting mixture underwent an 8-hour grinding process using an agate mortar and pestle to achieve homogeneity. Subsequently, the powder was sintered at 900 °C for 4 hours in the muffle furnace, a crucial step in the synthesis to integrate zinc into the alumina lattice structure.

The prepared samples underwent a rigorous characterization process to assess their physical properties. This included analysis using advanced techniques such as X-ray diffractometer (Bruker D8 Advance), Scanning Electron Microscope (SEM), Transmission Electron Microscope (TEM), Surface Area Analysis (BET, AutosorbiQ, Quantachrome USA) and diffuse reflectance spectrometer (UV/Vis spectrometer, Perkin Elmer). These characterization methods provide valuable insights into the crystalline structure, morphology, and optical properties of the synthesized materials. In addition to physical characterization, the electrochemical properties of the samples were thoroughly investigated using sophisticated instruments. An AC impedance analyzer was utilized to study the materials' impedance behavior, providing valuable information on their conductivity and charge transfer kinetics. The Galvanostatic Charge-Discharge (GCD) test allowed for the assessment of the materials' charge storage capabilities under specific current conditions. Furthermore, cyclic voltammetry (CV) was employed to analyze the materials' electrochemical stability and capacitance behavior over multiple cycles. A SC device of asymmetric type has been constructed to study the electrochemical analysis of the Asymmetric SC device.

3 Result and Discussion

3.1 Structural Properties

The diffraction pattern depicted in Figure 1 confirms the formation of single-phase γ-Al_2O_3 nanoparticles in the initial layer. The peaks were meticulously analyzed and fitted using the Fityk software [30]. For pure alumina, the peaks obtained align perfectly with the JCPDS #02-1420 reference, indicating the successful synthesis of pure alumina nanoparticles. However, the diffraction pattern for zinc-doped Al_2O_3 exhibits an intriguing enhancement in peak intensities common to both Al_2O_3 and zinc oxide nanoparticles. Specifically, the diffraction patterns of the 5% and 7% zinc-doped alumina nanoparticles reveal additional peaks corresponding to zinc oxide and metallic zinc clusters, notably at 33° [31] and 54° [16], respectively. This phenomenon is attributed to the positioning of zinc and excess oxygen ions within the alumina lattice. It is noteworthy that the highest intensity peak shifts to higher 2θ

values with an increase in the dopant concentration. This shift is attributed to the lattice stress resulting from the alternate arrangement of Al and Zn ions, forming an intercalative structure [32]. Moreover, the average crystallite size, calculated using the Scherrer formula with a k value of 0.98 [33-35], decreases from 9 nm to 5 nm with increasing dopant concentration. Furthermore, the lattice strain is observed to increase from 5 x 10^{-3} to 7 x 10^{-3}, accompanied by an increase in dislocation density with the rising dopant concentration. The presence of diffraction peaks related to zinc, the shift in diffraction angles to higher values, and the increased lattice strain collectively confirm the successful incorporation of Zn ions within the Al oxide lattice. The variation in the ionic radii of host (53 pm) and dopant ions (74 pm) along with the observation of decreased average crystallite size confirms the formation of trapping centers. It also suggests that the intercalation of zinc ions in the lattice of alumina hinders the growth of alumina structure leading to decrease in average crystallite size [36].It also emphasizes the probability of having enhanced energy storage capacity as literature reports states the correlation of smaller crystallite sizes with higher and stable electrochemical properties[15, 37, 38]. These detailed structural analyses provide valuable insights into the unique properties of zinc-doped alumina nanoparticles. The observed shifts in diffraction patterns, changes in crystallite size, and lattice strain variations elucidate the structural modifications induced by zinc doping. This enhanced understanding of the material's structural evolution is pivotal for harnessing its potential for advanced energy storage applications.

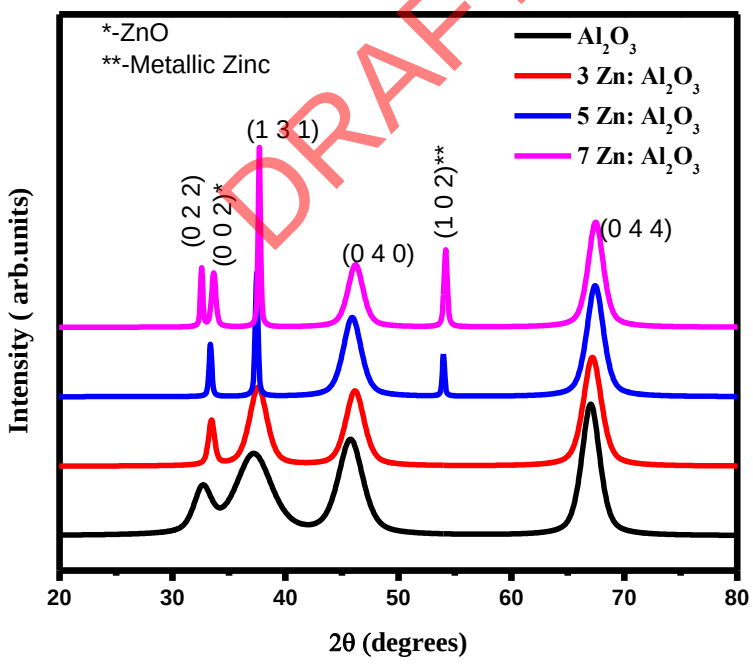

Fig. 1 Diffraction pattern for pure Al_2O_3, 3%,5%, 7% Zinc doped Alumina Nanoparticles arranged from bottom to top layer.

3.2 Morphological Properties

The SEM morphology of Zn-doped Al_2O_3 nanoparticles shows distinct changes as the Zn doping concentration increases from 3% to 7% as shown in Figure 2(a-c). At 3% Zn doping, the particles are relatively small and exhibit a non-uniform distribution. The particles are

mostly spherical with few agglomerations, indicating a somewhat controlled doping process. There are noticeable pores within the particles, suggesting moderate porosity. When the Zn doping is increased to 5%, the particles become slightly larger with a more noticeable increase in agglomeration and non-uniform distribution. The particles maintain a spherical shape, but there are more irregularities on the surface, suggesting the incorporation of more Zn. The porosity appears to increase, with more prominent and larger pores within the particles. At 7% Zn doping, the particles are significantly larger with pronounced agglomeration and a highly non-uniform distribution. The particles are less distinct in shape, with many irregular and rough edges, indicating that excessive Zn doping leads to structural changes and increased clustering. The porosity is even more significant at this concentration, with extensive pore networks throughout the particles. The SEM micrographs of all Zn doped alumina taken at different magnifications are attached in Supplementary Fig. S1.(a-c). As the Zn doping concentration increases, there is a clear trend of increasing particle size, more agglomeration, and a shift from uniform spherical shapes to more irregular and rough structures, with a consistently non-uniform distribution. Additionally, the porosity of the particles increases with higher Zn doping, leading to more extensive and pronounced pore networks.

Confirming the elemental composition, the energy-dispersive X-ray spectroscopy (EDS) spectra in Figure 2d affirm the presence of Aluminium, Zinc, and Oxygen in stoichiometric quantities. Additionally, the EDS spectra reveal an excess amount of oxygen in the zinc-doped alumina nanoparticles. This excess oxygen can influence the material's properties and behaviour, potentially impacting its performance in energy storage applications [39, 40].

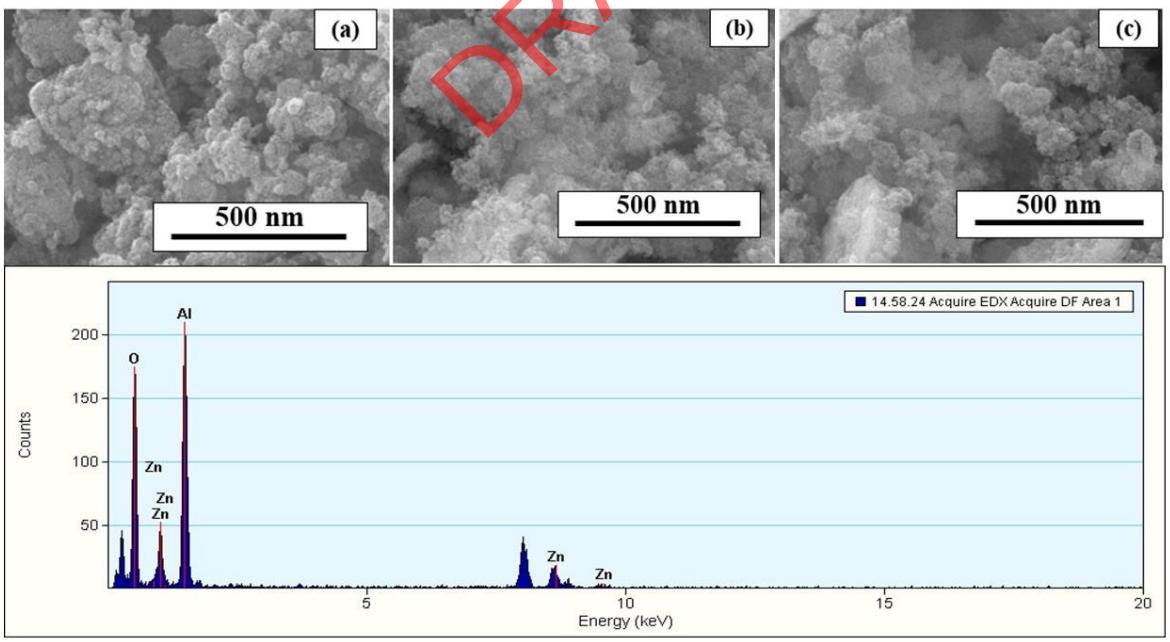

Fig. 2 SEM morphology of (a) 3% Zn doped Al_2O_3 (b) 5% Zn doped Al_2O_3 and (c) 7% Zn doped Al_2O_3 nanoparticles and (d) EDS spectra of zinc doped alumina nanoparticles.

Moving to the transmission electron microscope (TEM) images shown in Figure 3(a-c), the porosity of the 5% zinc-doped alumina nanoparticles quantified using Image J software,

is yielding a porosity value of 11.097%. This porosity plays a crucial role in enhancing the material's capacity for charge storage, a vital aspect for energy storage applications. Moreover, the interplanar spacing has been determined from the high-resolution TEM (HRTEM) image in Figure 3(d). The selected area electron diffraction (SAED) results in Figure 3(e)& 3(f) show distinct dotted rings, confirming the crystalline phase formation of gamma alumina [41]. This observation further reinforces the single-phase formation of zinc-doped alumina, as indicated by the morphological studies. Pure gamma alumina exhibits an interplanar spacing of 0.198 nm, while the 5% Zn-doped Al_2O_3 displays an increased interplanar spacing of 0.262 nm. This slight increase in interplanar spacing provides ample room for the dopant to facilitate intercalation[42, 43], creating spaces for the storage of charges[43], thus enhancing its suitability for energy storage applications.

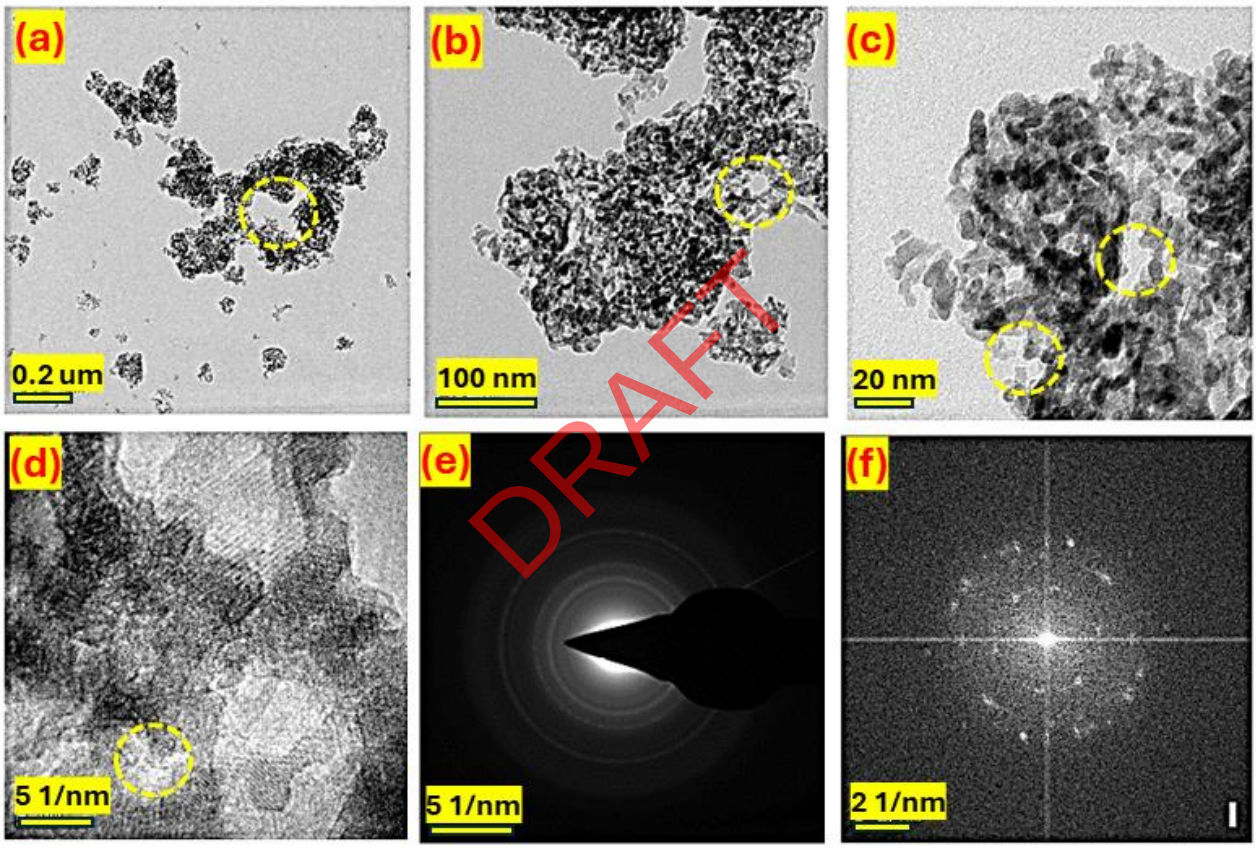

Fig. 3(a-c) TEM micrograph of 5% Zn doped Al_2O_3 (d) HR-TEM micrograph of 5% Zn doped Al_2O_3 (e-f) SAED image of 5% Zn doped Al_2O_3 nanoparticles

3.3 Optical Properties

The absorbance and reflectance spectra exhibit maximum absorbance and minimum reflectance within the visible region of the light spectrum. Analysis using Tauc's plot (Fig. 4), derived from the reflectance spectra, using KubelkaMunk equation[44]reveals band gaps of 1.48 eV for pure gamma alumina, 3.01 eV, 4.86 eV, and 4.21 eV for 3%, 5%, and 7% zinc doping concentrations in alumina, respectively, as depicted in Figure 5(a-d). The increase in the band gap correlates the formation of trapping centers due to intercalation of Zn ions in the

host lattice leading to Burstein-Moss effect on increase in concentration of Zn ions [45]. Also, it is seen in literature that band gap increased for the host lattice on doping with zinc [46, 47].Notably, band gaps falling within the range of 3 eV to 5 eV categorize these materials as wide band gap semiconductors, with a high potential for SC behavior [48]. This wide band gap characteristic is significant, as it enhances the stability of energy storage density [49-51]. Essentially, materials with wide band gaps can store energy for longer durations without significant leakage or dissipation. In essence, the observed band gaps in the zinc-doped alumina nanoparticles suggest their suitability for SC applications. The wide band gap semiconductor behavior not only indicates potential for efficient energy storage but also underscores the stability required for extended energy retention. These characteristics align well with the demands of advanced energy storage technologies, highlighting the promise of these materials for future applications.

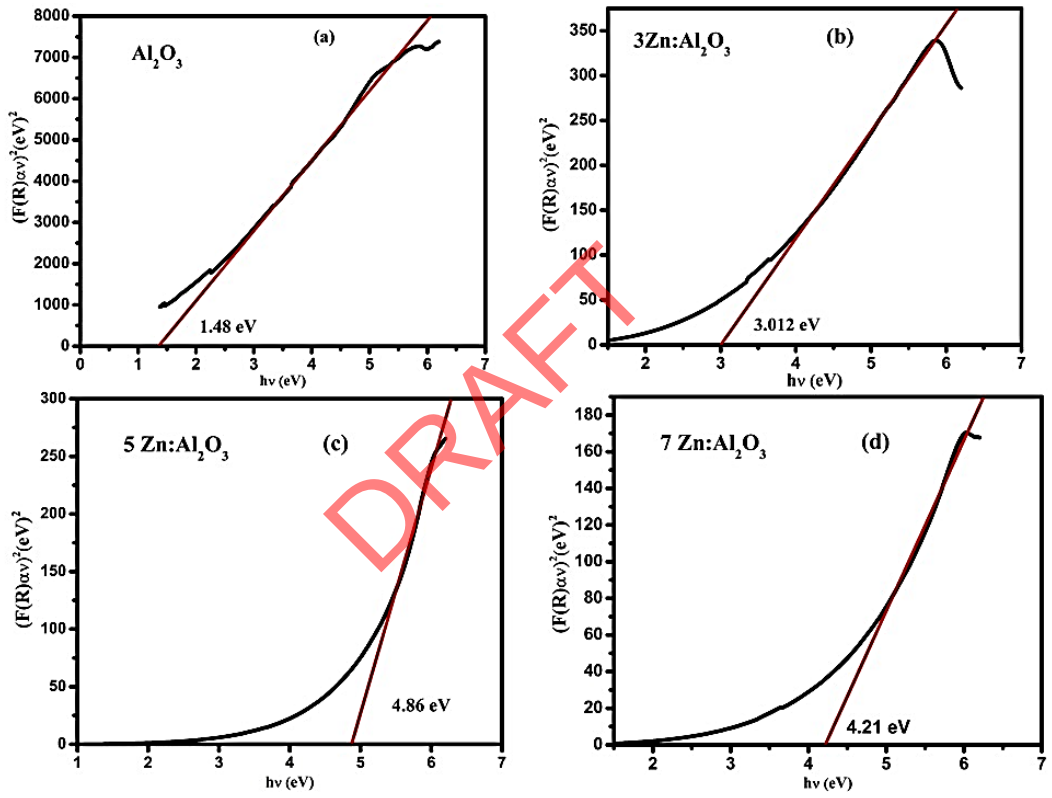

Fig. 4(a-d) Optical Band gap analysis of Zn doped Alumina nanoparticles.

3.4 XPS studies

The presence of elements and the valence state of 5% Zn-doped Al_2O_3 is being analysed via XPS study, with the results depicted in Fig. 5 (a-e). The observed peaks at ~73 eV, ~1020 eV, and ~530 eV correspond to elements such as Al, Zn, and O in the samples, as confirmed by the wide spectrum[52]. Additionally, the presence of carbon (C) 1s peak, is attributed to hydrocarbon contamination on the sample surface introduced from the laboratory environment. Thus, the observed C 1s peak serves as an energy reference for determining the peak positions of core-level spectra. For a deeper understanding of the valence state in Aluminium and Zinc ions within the samples, high-resolution spectra of Al 2p and Zn 2p energy levels has been analysed, as depicted in Fig. 5b-d.In Fig. 5b, the narrow scan spectra of Al 2p for the 5% Zn-

doped Al_2O_3 sample are presented. After de-convoluting, the Al 2p peak is fitted into a single peak at 73.7 eV, corresponding to the Al^{3+} oxidation state of the sample[52].Fig. 5c reveals the de-convoluted Zn 2p peak into two peaks located at 1019.2 eV and 1042.4 eV, corresponding to the Zn $2p_{3/2}$ and Zn $2p_{1/2}$ peaks, respectively. These peaks are being fitted using a Gaussian-Lorentzian product function after Shirley-type background subtraction. The spin-orbital splitting energy of the Zn 2p doublet is determined to be 23.2 eV, indicating an oxidation state of Zn^{2+} in the 5% Zn-doped Al_2O_3 sample[53]. Fig. 5d displays the O 1s XPS peak of the 5% Zn-doped Al_2O_3 sample, which is well-fitted into a single peak situated at a binding energy of 530.59 eV. This peak at 530.59 eV attributes to the contribution of crystal lattice oxygen. Based on these results, XPS observations confirm that no additional/impurity phases are formed, further supporting the EDS and XRD results.

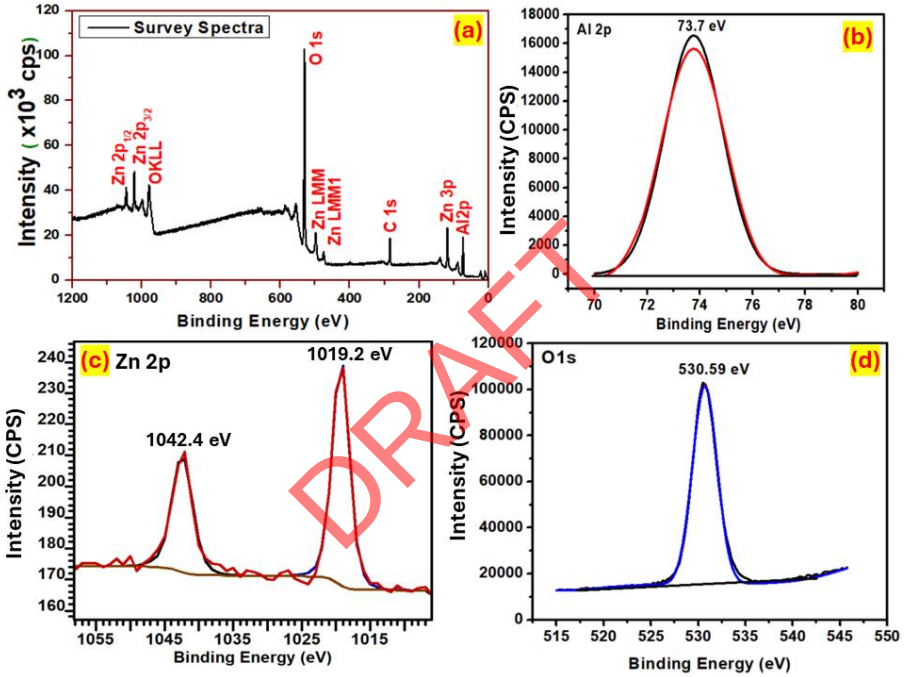

Fig. 5a Survey scan and Narrow scan spectrum of Al 2p (b), Zn 2p (c) and O 1s (d) for 5% Zn doped Al_2O_3nanoparticles.

3.5. Surface Area- BET analysis

Extensive studies are conducted to analyze the pore distribution and surface areas of the fabricated electrodes (Al2O3 and 5% Zn-Al2O3) using the BET (Brunauer-Emmett-Teller) technique. The N_2 adsorption-desorption isotherms, shown in Figure 6, reveals a type-IV hysteresis loop at high pressure, indicating mesoporous behavior in all the electrodes. The BET surface area of the Al_2O_3 electrode is found to be approximately 267.78 m^2/g, while the 5% Zn-Al_2O_3 sample has a surface area of 304.52 m^2/g. This indicates that the incorporation of Zn ions increases the specific surface area of the material. Pore size distribution analysis shows a narrow range of pore sizes, confirming the presence of mesopores that provide abundant sites for electrochemical reactions. Specifically, the 5% Zn-Al_2O_3 electrode material exhibits a large surface area and mesopores with an average size of 6.42 nm, compared to 1.42 nm for Al_2O_3. This enhanced porosity and increased surface area are conducive to improved electrochemical

performance, potentially leading to higher capacitance and better cycling stability in SC applications. Moreover, the enhanced mesoporosity in the Zn-doped samples may facilitate more efficient ion transport and accessibility, thereby boosting the overall electrochemical activity and energy storage capacity of the electrodes.

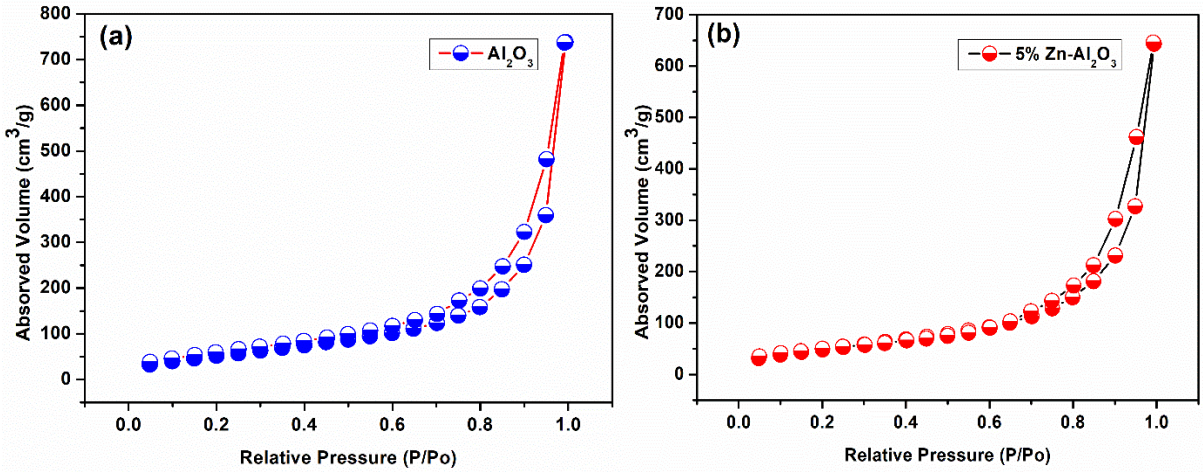

Fig. 6. N_2 absorption-desorption isotherms of the as-prepared electrodes (Al_2O_3 and 5% Zn-Al_2O_3) samples.

3.6 Electrochemical measurements

The suitability of pure and Zn doped Al_2O_3 nanoparticles as energy storage materials are checked by electrochemical studies like CV, GCD and impedance measurements. These characterizations are carried out using three electrode configuration models having 2M KOH aqueous solution between an operating potential ranges of -0.2 to 0.4 V. The optimization of the operating potential range for the nanoparticles, cyclic voltammetry is performed on them. It also helps to analyze the nature of charge storage mechanisms in the pure and zinc doped Al_2O_3 nanoparticles. A 2M KOH aqueous solution as the electrolyte for this experiment for several reasons, at first, high ionic conductivity: KOH is known for its high ionic conductivity, which is essential for the efficient performance of (SCs). The high ionic mobility in KOH solutions facilitates faster charge/discharge cycles. The secondary reason is stability: KOH provides a stable electrochemical environment, which is crucial for ensuring the long-term stability and performance of the electrode materials. Finally, the compatibility with alumina: KOH is particularly effective in enhancing the electrochemical properties of alumina-based materials. The alkaline environment helps in achieving better electrochemical performance through improved pseudocapacitive behaviour. Moreover, KOH is a widely used electrolyte in SC research, allowing for easier comparison of results with existing literature. Its properties are well-documented, providing a reliable basis for evaluating the performance of zinc-doped alumina electrodes. The results of CV measurements of all the electrodes are displayed in Figure 7.

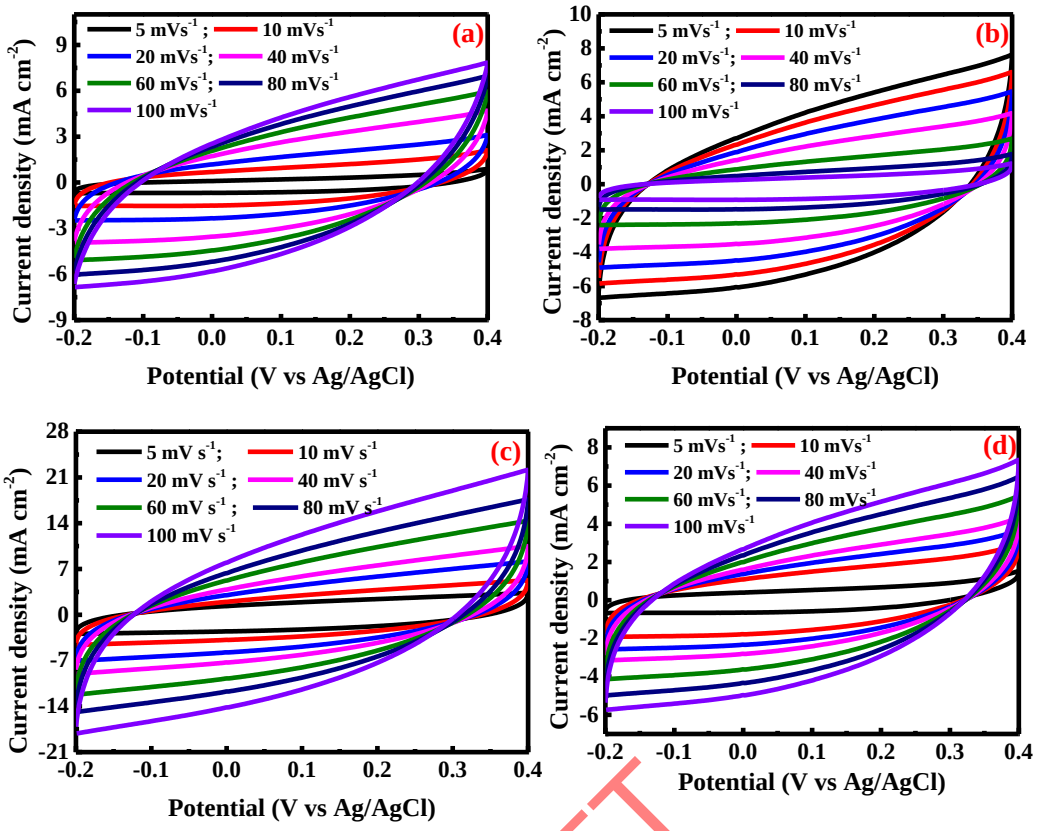

Fig 7. CV curves at different scan rates of (a) Al_2O_3 (b) 3 wt.% of Zn doped Al_2O_3 (c) 5 wt.% of Zn doped Al_2O_3 (d) 7 wt.% of Zn doped Al_2O_3.

The voltammograms have been observed in quasi-rectangular shape for all the electrodes scanned at a scan rate of 5 mV s^{-1}as shown in Figure 8a. Along with that, there is an observation of increase in area under CV curve for the Zn doped Al_2O_3 nanoparticles (Figure 8a and 8b). This suggests that the enhancement of electrochemical performance of Zn doped Al_2O_3electrodes tos tore energy via intercalative pseudocapacitance behavior [54]. Among the CV curves, the voltammogram of Al_2O_3 doped with 5 wt.% Zn electrode encloses the larger area than the other electrodes signifying its potential in the storage capacity. The specific capacitance of prepared electrodes is calculated using the relation 1[55, 56],

$$C_S = \frac{\int I \, dV}{2 \, m \, \nu \, V} \qquad 1$$

Where, C_S represents the specific capacitance (F g^{-1}), $\int I \, dV$ is area under voltammogram (A V), m represents the mass of electroactive material (mg), ν and indicates the scan rate (mV s^{-1}) and V is the potential window (V). The estimated specific capacity for the electrodes of pristine Al_2O_3, 3, 5 and 7 wt.% Zn doped $Al_2O_3$are found to be 130, 244, 638 and 281 F g^{-1} respectively. Notably, 20.4 % capacitance is increased on addition of 5 wt.% of Zn in Al_2O_3 electrode, and it is found to be suitable concentration for increasing the electrochemical performance of Al_2O_3. The reduction and oxidation reactions, the overall pseudocapacitive reaction for γ-Al_2O_3 can be represented as:

$$Al_2O_3+3H_2O+3e^- \rightleftharpoons 2Al(OH)_3 \qquad 2$$

Furthermore, the quantum of charges stored via surface capacitance and intercalative capacitance has been estimated using Dunn's method. Mathematically, the total capacitance can be represented as [57],

$$Q_T = Q_S + \frac{\text{constant}}{\sqrt{\nu}} \qquad 3$$

Where, Q_T is total charges stored (F g^{-1}), Q_S represents charges stored via surface capacitance (F g^{-1}) and ν indicates the scan rate (mV s^{-1}). Figure 8c displays the linear response between specific capacitance and inverse square root of scan rate. The Y intercept of Fig. 8c, while extrapolating the straight line, gives the quantum of surface capacitance.

Herein, from Fig. 8d, it can be observed that the surface capacitance of pristine Al_2O_3 electrode decreases on addition of Zn, signifying the impact of the presence of Zn^{2+} in the interstitial position forming intercalating layer. The intercalative arrangement of Zn^{2+} tend to form Van der Waals kind of bonding between two like charges of Zn^{2+} and Al^{3+} lattice[58]. This correlates with the entering of electrolytic ions into the electrode surface and bulk in large amount due to greater surface area of the electrodes in form of Zn^{2+} and Al^{3+} ions. But the presence of like charges in the interstitial and host lattice position also form a high potential barrier between Al^{3+} and Zn^{2+} ion. This potential barrier hinders the flow of electrolytic free ions from one position to another leading to reduction in the flow of current and increase in the storage of current density. Thus, the charges can be stored for a longer duration until higher potential is applied because of the intercalation phenomenon[59] making the Zn doped Al_2O_3 electrode an efficient energy storage candidate.

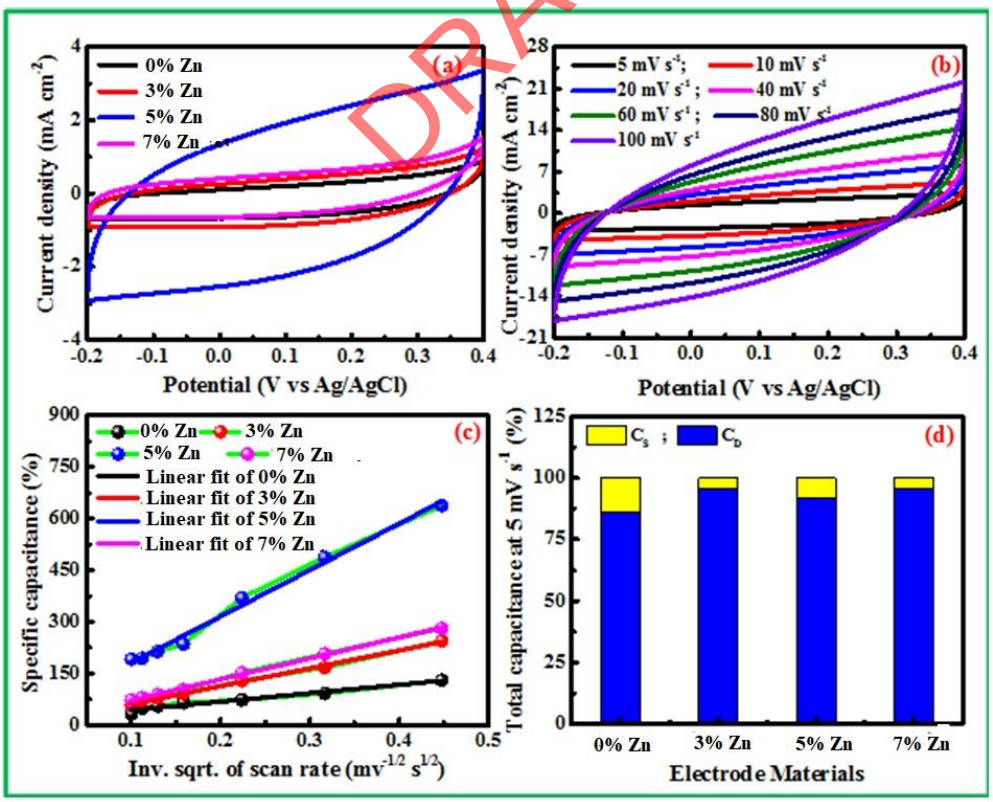

Fig. 8(a) CV curves of at 5 mV s^{-1}, (b) CV curves of 5 wt.% of Al doped ZnO, (c) C_S *versus* $\nu^{-1/2}$ and (d) Percent of surface and diffusion capacitance of ZnO and Al doped ZnO electrodes.

This phenomenon is also supported by the observation of non-linear decrease of surface capacitance with the increase of Zn concentration in Al_2O_3 electrodes (Figure 8d). In detail, the quantum of surface contribution decreases for the Al_2O_3 electrodes consisting of 3 and 7 wt.% of Zn. While, a significant impact of surface-controlled process is seen in 5 wt.% Zn doped Al_2O_3 electrode that can be attributed to superior charge storage performance.This observation suggests that the addition of zinc alters the surface properties of the electrode, influencing its capacitance characteristics. Non-linear behavior in capacitance indicates complex interactions between the electrode material and the electrolyte, which can be further explored to optimize the electrode design for better energy storage performance. Besides, the prepared electrodes are being employed to investigate its capability of charging and discharging at constant specific current within a potential of -0.2 to 0.4 V. GCD curves of all the electrodes are displayed in Figure 9.

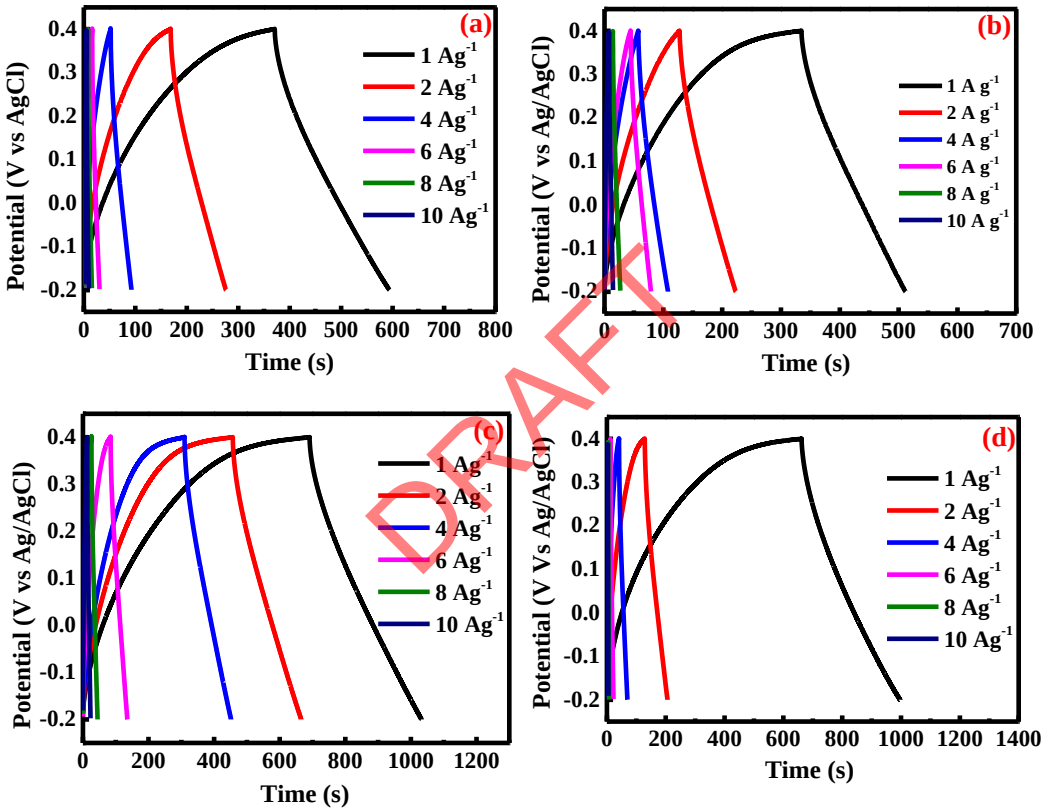

Fig 9. GCD curves of (a) Al_2O_3 (b) 3 wt.% of Zn doped Al_2O_3 (c) 5 wt.% of Zn doped Al_2O_3 (d) 7 wt.% of Zn doped Al_2O_3at different Ag^{-1}.

All the electrodes display a quasi-linear charge-discharge process, and it may be primarily attributed to ion intercalation phenomena which is consistent with the results obtained in CV analysis. Figure 9a demonstrates the GCD curves of all the electrodes recorded at a specific current of 1 A g^{-1}. Among the various electrodes, 5 wt.% Zn doped Al_2O_3 encircles the large area under charge and discharge curve signifying the excellent electrochemical performance.Figure 9b shows the GCD curves of Al_2O_3 containing 5 wt.% Zn and the area of the curve is decreasedwith the increase of specific current. This is explained based on the lagging of time for the electrolyte ions to intercalate into the matrix of electrodes. The specific

capacity of the Al_2O_3 and Al_2O_3/Zn composite electrodes are being estimated using the equation 4 [55, 56],

$$C_S = \frac{2I \int V \, dt}{m \, V^2} \qquad 4$$

Where, I, specific current (A g^{-1}), $\int V \, dt$, area under discharge curve (V s), m, mass of electroactive material (mg) and V, potential window (V). The specific capacity of 798, 1864, 1237 and 919 F g^{-1} is estimated at a specific current of 1 A g^{-1} respectively for the electrodes of pristine Al_2O_3, 3, 5 and 7 wt.% Zn doped Al_2O_3 as shown in Figure 10a.

Among these, the electrochemical performance of Al_2O_3 consisting of 5 wt.% Zn is pretty good due to the optimal contribution of surface and intercalation capacitance. Moreover, the lifespan test of 5% Zinc doped Al_2O_3 electrode is being examined upon 10000 continuous charge discharge cycles. The performance has been recorded for each 250 cycles by estimating retention from its initial value under 10 mA cm^{-2} current density using GCD technique. The varying retention upon increasing GCD cycles are shown in Figure 10b. The performance of pristine Al_2O_3 electrode is found to decrease on increasing the cycles whereas the 5 wt.% Zn doped Al_2O_3 shows increasing trend of retention in the 250th cycle and the same is continued until the cycle reaches to 500th cycle. The retention is decreased on further increasing the GCD cycles and finally 5% Zn doped Al_2O_3 electrode retains 92% of its initial value even after 10000 GCD cycles as shown in Fig. 10b.

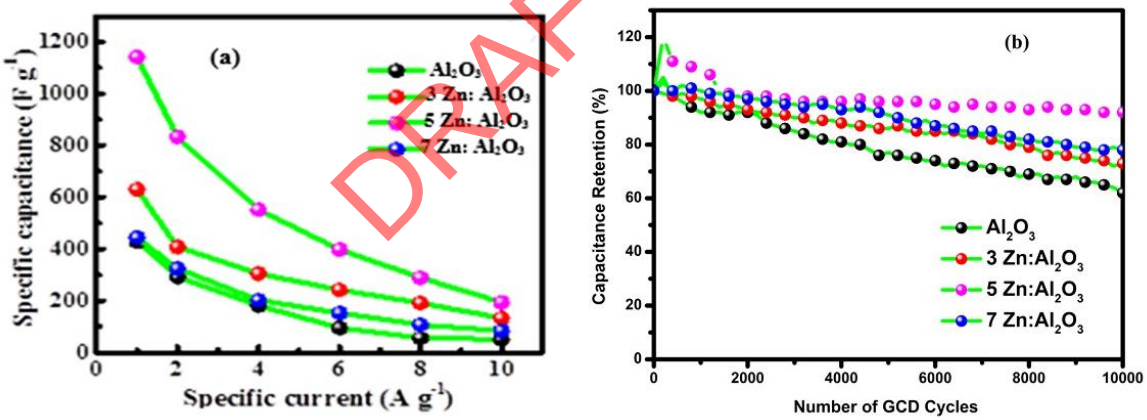

Fig. 10(a) C_S *versus* specific current and (b) lifespan test of Al_2O_3 and 5 wt.% Zn doped Al_2O_3 electrodes

The AC impedance analysis is further utilized to diagnose the impedance associated with the intercalative performance of prepared electrode materials for frequencies ranging from 100 mHz – 100 kHz with an amplitude of 5 mV. The obtained impedance spectra are being fitted using modified Randle's circuit (inset of Fig10a) and it is shown in Fig11a. The results of impedance analysis are being examined in the form of Nyquist plot and log |Z'| versus log (1/ω) as shown in Fig. 11b. Moreover, Figure11a shows the existence of semi-circular Nyquist plot in high frequency region which indicates the charge transfer controlled process. The solution resistance of 3.89, 2.14, 1.3 and 1.74 Ω and charge transfer resistance of 3.65, 1.48, 0.8 and 1.22 Ω for the respective electrodes of Al_2O_3, 3, 5 and 7 wt.% Zn doped Al_2O_3has been obtained from the diameter of semi-circular region and the X-intercept value, respectively.

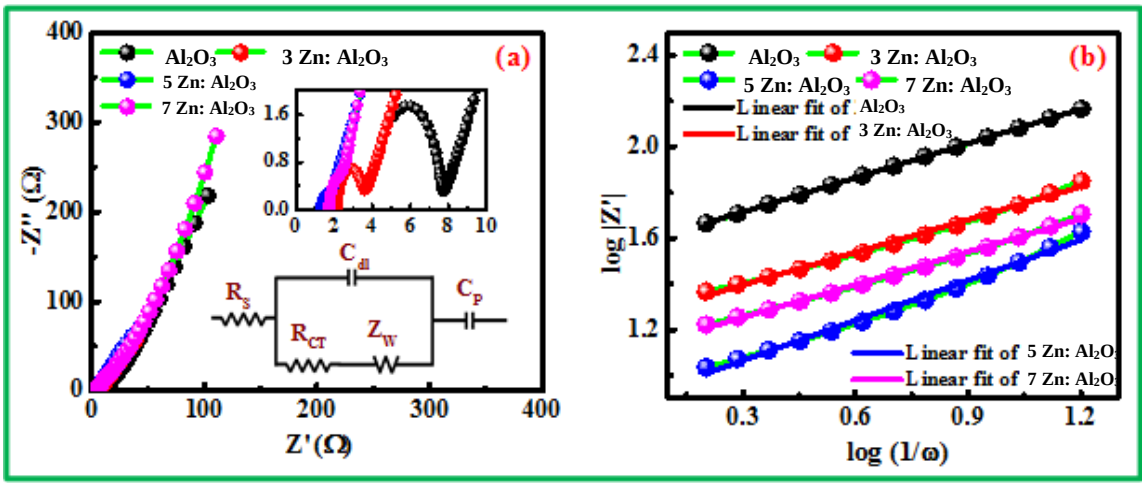

Fig 11. (a) Nyquist plot, (Inset of Figure 10 (a) Modified Randle's circuit) and (b) log |Z'| *versus* log (1/ω).

The low charge transfer resistance of 0.8 Ω is obtained for 5 wt.% Zn doped Al_2O_3 accounting outstanding charge storage performance. Besides, inclined straight line is being seen in low frequency region and it is indicative of intercalation process of electrolyte ions. The diffusion coefficient was estimated using the relation in equation 5,[57, 60, 61]

$$D = \frac{R^2T^2}{2A^2n^4F^4C^2\sigma^2} \quad \cdots \quad 5$$

where, R is the gas constant (8.314 J mol^{-1} K^{-1}); T is the temperature (295 K), A represents the surface area (1 cm^2); n is the number electrons transferred; F indicates the Faraday constant (96485 C mol^{-1}); C specifies the molar concentration of OH^- ions (6×10^{-3}mol cm^{-3}) and σ designates the Warburg coefficient[62]. The value of σ can be obtained from the Y intercept of straight line fitted between log |Z'| versus log (1/ω) (Figure 11b). The obtained value of sigma for the electrodes of Al_2O_3, 3, 5 and 7 wt.% Zn doped $Al_2O_3$are 36.3, 17.8, 7.76, and 12.9 Ω. This led to yielding the diffusion coefficients such as 0.4, 1.7, 8.9 and 3.2×10^{-12} cm^2 $s^{-1}$for Al_2O_3, 3, 5 and 7 wt.% Zn doped Al_2O_3 electrodes, respectively. Herein, the Al_2O_3 electrode doped with 5 wt.% Zn is endowed with highest diffusion coefficient of 8.9×10^{-12} cm^2 s^{-1} signifying that the presence of zinc and aluminum could provide the efficient active cites for the intercalation of electrolyte ions accounting its superior electrochemical performance.

The enhanced electrochemical activity in Zn-doped Al_2O_3 can be attributed to several key factors: (i) Improved Electrical Conductivity, (ii) Increased Surface Area and Porosity, and (iii) Enhanced Redox Activity. The electrical conductivity is improved by inclusion of additional charge carriers due to Zinc doping. Similarly, the insertion of Zinc in the lattice of alumina also influences the porosity and surface area as confirmed by the BET scan and other morphology studies. Zinc ions has the tendency to initiate reversible redox reactions that majorly contributes to pseudocapcitance charge storage mechanism. The increased conductivity facilitates faster electron transport during the charge-discharge cycles and also the morphology change helps in creation of more active sites in the alumina lattice. These factors play a vital role in overall improvement of electrochemical performance reporting improved charge storage and cyclic stability. Thus, Zinc doping can improve the structural stability of Al_2O_3, preventing degradation and maintaining the integrity of the electrode material over

extended cycling. This stability is crucial for achieving high specific capacities and long-term cycling performance.

Table 1: Comparison of electrochemical characteristics of Zn: Al_2O_3 with other reported materials.

S. No.	Electrode materials	Synthesis method	Morphology	Potential window V	Specific capacity F g^{-1}@A g^{-1}	Stability % @ cycles	Ref
1	Zr/ZnO	Chemical coprecipitation method	Porous cloud network-like structure	0 – 0.68	518@1	94 @ 5000	[8]
2	V/Ce/NiO/C	Sol-gel	Nanoparticles	-0.05 –0.65	1719 @2	98.21@5000	[9]
3	MnSe/$SrZrO_3$	Pechini Route	Nanocomposite	-0.1–0.65	1204 @1	95.2@3000	[14]
4	CTAB/NiO	Sol-gel	Nanoflower	-0.05 – 0.55	397@1	86 @ 1600	[12]
5	Er/Ce/Nd_2O_3	Sol-gel	Plate like	-0.01 – 3.1	1319 @ 5	96@1000	[13]
6	V/La/TiO_2	Sol-gel	Nanospheres	0.1 – 0.65	803 @ 1	93 @ 1000	[11]
7	Ce/Ho/TiO_2	Sol-gel	Nanoparticles	0.1 – 0.5	1714 @ 2	99.28 @ 5000	[10]
8	Al/ZnO	Green synthesis	Nanoparticles	-0.2 – 0.4	1162 @ 1	92 @ 10000	Present work

3.7 Asymmetric Supercapacitor Device Characteristics

The adoptability of Zn-doped Al_2O_3 nanoparticles in commercial SC devices has been analysed by assembling of an asymmetric type (ASSC). The ASSCs have combination of one electrode categorized in EDLC material and another electrode categorized in pseudocapacitive material [63]. In the present work, ASSCs device is comprised with an electrode made of 5% Zn doped alumina attributing pseudocapacitance, another electrode as activated carbon(1100 m^2/g, SigmaAldrich, India) attributing to EDLC effect[64] and a polypropylene film (Celgard, 2400) acting as separator. The electrochemical feature of this asymmetric system is investigated in 2 M KOH electrolyte.

The energy storage features of Zn-doped Al_2O_3 base asymmetric device is presented in Fig. 12. The CV curves at different scan rats of the full cell device (Zn- Al_2O_3/2MKOH//AC) presented in Fig.12a shows the quasi rectangular shape. It indicates the dominancy of EDLC behaviour in the device. The GCD profiles of Zn- Al_2O_3//2MKOH//AC device is shown in Fig. 12b. The nonlinear GCD profiles indicate the influence of Faradaic process in the electrolyte ion intercalation and de-intercalation. The specific capacitance values are estimated for Zn-Al_2O_3//2MKOH//AC using GCD profiles. The calculated specific capacitance values are 175, 165, 153, 89 and 51 F $g^{-1}$for the current rates of 2, 4, 6, 8 and 10 A g^{-1}. Another important supercapacitive feature is the cyclic stability which contributes maximum in the overall efficiency of any SC device. This device reports a good cyclic stability of 84% of initial capacitance after 5000 repeated charge discharge cycles. So, a better sustainability has been attained using Zn doped alumina as electrode [65, 66].

The energy density and power density of the as fabricated Zn- Al_2O_3//2MKOH//AC device are estimated using the following formulae.

$$E = \frac{C(\Delta V)^2}{7.2} \ldots\ldots\ldots\ldots (6)$$

$$P = \frac{3600E}{t} \ldots\ldots\ldots\ldots (7)$$

Here, C (Fg^{-1}) is the capacitance, ΔV (V) is the potential window, P (WKg^{-1}) is the power density, E ($Whkg^{-1}$) is energy density and t (s) is the time. All the parameters are derived using discharge capacitance and used potential window of the GCD analysis. The estimated energy density is obtained as 47.63 W h kg^{-1} at a power delivery rate of 996.9 W kg^{-1}. The obtained energy density is found to be enhanced with respect to already reported results for various alumina composition electrodes [66].

The resistive and capacitive features of Zn- Al_2O_3//2MKOH//AC device is analysed using EIS measurements and respective Nyquist plot is presented in Fig. 12c. The equivalent circuit used in electrochemical data analysis in EIS measurement is shown in supplementary fig. S2. From the Nyquist plot, the X-axis intercept gives the solution resistance (R_S) and the diameter of the semicircle gives the charge transfer resistance (R_{CT}) values. The R_S and R_{CT} obtained are 16Ω and 18 Ω respectively.

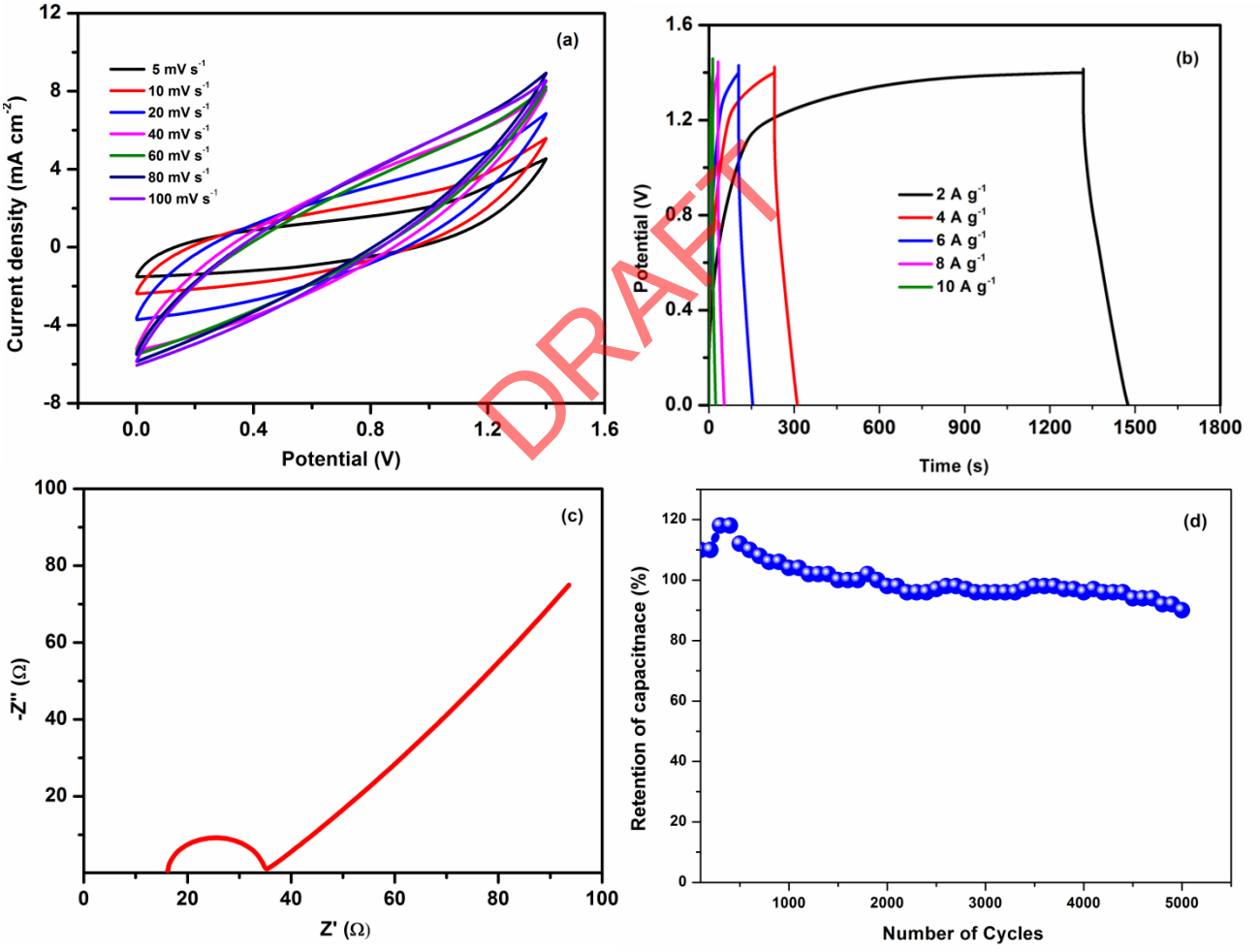

Fig. 12 Zn- Al_2O_3//2MKOH//AC ASSC. (a) CV curves at different scan rate. (b) GCD profiles at various current rates. (c) Nyquist plot (d) Cyclic stability measurements.

4 Conclusion

In conclusion, zinc-doped alumina nanoparticles is a promising candidate as an alternative to Li-ion batteries. Their lightweight nature is ideal for SC devices. The strategic positioning of Zn^{2+} ions create charge trapping centers for enhanced energy storage. Achieving a specific capacitance of 1237@1 Ag^{-1} highlights their potential. Zinc doping improves stability by 92% over 10000 cycles. The low charge transfer resistance of 0.8 Ω for 5 wt.% Zn-doped Al_2O_3 indicates outstanding charge storage performance. The diffusion coefficients for Al_2O_3, 3%, 5%, and 7% Zn-doped Al_2O_3 are 0.4, 1.7, 8.9, and 3.2×10^{-12} cm^2 s^{-1}, respectively. Notably, the 5% Zn-doped Al_2O_3 electrode exhibits the highest diffusion coefficient of 8.9×10^{-12} cm^2 s^{-1}, indicating efficient active sites for electrolyte ion intercalation. The asymmetric SC device comprising zinc doped alumina as one of the electrodes enhanced energy storage density, outstanding charge storage performance, better cyclic stability over 5000 cycles and superior electrochemical behavior. The present content highlights the contribution of potential barriers and intercalation phenomena to making Zn doped Al_2O_3 electrodes efficient for energy storage applications. These aspects are supported by experimental observations, including changes in surface capacitance with varying zinc concentrations, which provide insights into the material's electrochemical behavior and performance.They hold promise for next-generation energy storage technologies.

Acknowledgement:

Authors are grateful to VIT-Vellore for providing the XRD facility and Diffuse reflectance spectroscopy facility for the studies. Authors are thankful to King Khalid University, Saudi Arabia for performing XPS and Dr MCET for the electrochemical studies of our samples.

Data Availability:

Data sets generated during the current study are available from the corresponding author on reasonable request.

References

[1] M.E. Glavin, W.G. Hurley, Solar energy, 86 (2012), pp. 3009-3020.
[2] K. Shrestha, S. Sharma, G.B. Pradhan, T. Bhatta, S.M.S. Rana, S. Lee, S. Seonu, Y. Shin, J.Y. Park, Nano Energy, 102 (2022), p. 107713.
[3] M.S. Son, Journal of the Semiconductor & Display Technology, 20 (2021), pp. 25-28.
[4] Z. Duan, C. Hu, W. Liu, J. Liu, Z. Chu, W. Yang, L. Li, G. Shen, Advanced Materials Technologies, 8 (2023), p. 2300157.
[5] H. Sheng, L. Jiang, Q. Wang, Z. Zhang, Y. Lv, H. Ma, H. Bi, J. Yuan, M. Shao, F. Li, Science Advances, 9 (2023), p. eadh8083.
[6] Y.A. Kumar, C.J. Raorane, H.H. Hegazy, T. Ramachandran, S.C. Kim, M. Moniruzzaman, Journal of Energy Storage, 72 (2023), p. 108433.
[7] G. Xiao, J. Ju, M. Li, H. Wu, Y. Jian, W. Sun, W. Wang, C.M. Li, Y. Qiao, Z. Lu, Biosensors and Bioelectronics, 235 (2023), p. 115389.
[8] Y. Anil Kumar, G. Koyyada, T. Ramachandran, J.H. Kim, S. Sajid, M. Moniruzzaman, S. Alzahmi, I.M. Obaidat, Nanomaterials, 13 (2023), p. 1049.

[9] T. Munawar, A. Bashir, S. Sardar, M.S. Nadeem, F. Mukhtar, S. Manzoor, M.N. Ashiq, S.A. Khan, M. Koc, F. Iqbal, Journal of Energy Storage, 76 (2024), p. 109556.
[10] T. Munawar, S. Manzoor, K. Jabbour, M.U. Nisa, S. Sardar, F. Mukhtar, S.M. Osman, M.F. Esan, M.N. Ashiq, F. Iqbal, Journal of the Korean Ceramic Society, (2024).
[11] T. Munawar, S. Manzoor, F. Mukhtar, M.S. Nadeem, A.G. Abid, M.N. Ashiq, F. Iqbal, Journal of Materials Science, 57 (2022), pp. 11852-11870.
[12] T. Munawar, M. Shahid Nadeem, F. Mukhtar, S. Manzoor, M. Naeem Ashiq, F. Iqbal, Materials Science and Engineering: B, 284 (2022), p. 115900.
[13] T. Munawar, M. Shahid Nadeem, F. Mukhtar, S. Manzoor, M. Naeem Ashiq, M. Riaz, A. Hussain, F. Iqbal, Journal of Electroanalytical Chemistry, 920 (2022), p. 116614.
[14] A.W. Rabbani, T. Munawar, M.M. Alam, C.-F. Yan, M. Amanullah, F. Mukhtar, M.N. Ashiq, A. Khalid, N.N. Riaz, S.A. Khan, M. Koc, F. Iqbal, Ceramics International, 50 (2024), pp. 22884-22896.
[15] S. Suthakaran, S. Dhanapandian, N. Krishnakumar, N. Ponpandian, Journal of Physics and Chemistry of Solids, 141 (2020), p. 109407.
[16] E. Widyastuti, J.-L. Hsu, Y.-C. Lee, Nanomaterials, 12 (2022), p. 463.
[17] M.E. Şahin, F. Blaabjerg, A. Sangwongwanich, Energies, 15 (2022), p. 674.
[18] P.A. Shinde, Q. Abbas, N.R. Chodankar, K. Ariga, M.A. Abdelkareem, A.G. Olabi, Journal of Energy Chemistry, 79 (2023), pp. 611-638.
[19] H.H. Hegazy, S.S. Sana, T. Ramachandran, Y.A. Kumar, D.K. Kulurumotlakatla, H.S.M. Abd-Rabboh, S.C. Kim, Journal of Energy Storage, 74 (2023), p. 109405.
[20] P. De, J. Halder, C.C. Gowda, S. Kansal, S. Priya, S. Anshu, A. Chowdhury, D. Mandal, S. Biswas, B.K. Dubey, Electrochemical Science Advances, 3 (2023), p. e2100159.
[21] R.K. Gupta, Pseudocapacitors: Fundamentals to High Performance Energy Storage Devices, Springer Nature2023.
[22] K.D. Kumar, N. Roy, T. Ramachandran, I.K. Durga, M.S. Khan, Y.A. Kumar, S.S. Rao, S.W. Joo, Materials Science and Engineering: B, 306 (2024), p. 117444.
[23] T. Mo, Z. Wang, L. Zeng, M. Chen, A.A. Kornyshev, M. Zhang, Y. Zhao, G. Feng, Advanced Materials, 35 (2023), p. 2301118.
[24] M. Aalim, M.A. Shah, Vacuum, 210 (2023), p. 111903.
[25] J. Xu, X. Xiao, J. Zhang, J. Liu, J. Ni, H. Xue, H. Pang, Particle & Particle Systems Characterization, 34 (2017), p. 1600420.
[26] T. Ramachandran, F. Hamed, Journal of Physics and Chemistry of Solids, 121 (2018), pp. 93-101.
[27] T. Ramachandran, F. Hamed, Journal of Physics and Chemistry of Solids, 188 (2024), p. 111915.
[28] D. Nualsing, N. Pannucharoenwong, P. Rattanadecho, S. Echaroj, C. Benjapiyaporn, J. Benjapiyaporn, Energy Reports, 7 (2021), pp. 720-729.
[29] M. Appadurai, E.F.I. Raj, I. Jenish, Process Integration and Optimization for Sustainability, 6 (2022), pp. 211-222.
[30] M. Wojdyr, Journal of applied crystallography, 43 (2010), pp. 1126-1128.
[31] M. Shatnawi, A.M. Alsmadi, I. Bsoul, B. Salameh, M. Mathai, G. Alnawashi, G.M. Alzoubi, F. Al-Dweri, M.S. Bawa'aneh, Results in Physics, 6 (2016), pp. 1064-1071.

[32] R. Mondal, N.K. Mishra, T. Maiyalagan, A. Gupta, P. Singh, ACS omega, 6 (2021), pp. 30488-30498.
[33] P. Scherrer, Nach Ges Wiss Gottingen, 2 (1918), pp. 8-100.
[34] J.I. Langford, A.J.C. Wilson, Journal of applied crystallography, 11 (1978), pp. 102-113.
[35] V. Uvarov, I. Popov, Materials characterization, 58 (2007), pp. 883-891.
[36] D. Yu, S. Zhang, D. Liu, X. Zhou, S. Xie, Q. Zhang, Y. Liu, G. Cao, Journal of Materials chemistry, 20 (2010), pp. 10841-10846.
[37] C.-W. Huang, B.-J. Lin, H.-Y. Lin, C.-H. Huang, F.-Y. Shih, W.-H. Wang, C.-Y. Liu, H.-C. Chui, Nanoscale research letters, 7 (2012), pp. 1-6.
[38] J. Wang, J. Polleux, J. Lim, B. Dunn, The Journal of Physical Chemistry C, 111 (2007), pp. 14925-14931.
[39] X.-r. Li, Y.-h. Jiang, P.-z. Wang, Y. Mo, W.-d. Lai, Z.-j. Li, R.-j. Yu, Y.-t. Du, X.-r. Zhang, Y. Chen, New Carbon Materials, 35 (2020), pp. 232-243.
[40] L. Zhang, L. Song, X. Wang, C. Wu, S. Yu, Journal of Materials Science: Materials in Electronics, 33 (2022), pp. 1-11.
[41] X. Zhang, M. Honkanen, Y. Ge, S.-P. Hannula, E. Levänen, T. Mäntylä, NANOCRYSTALLINE γ-ALUMINA AND α-ALUMINA FROM BOEHMITE NANOFLAKES, 2008.
[42] Z. Chen, Q. Fan, M. Huang, H. Cölfen, Small, 19 (2023), p. 2300509.
[43] J. Wang, X. Li, Y. Xu, F. Duan, S. Yang, Z. Cao, Y. Dan, L. Chen, X. Cheng, Energy & Fuels, 35 (2021), pp. 3479-3489.
[44] D. Chakraborty, K. Shaik, Journal of Magnetism and Magnetic Materials, 486 (2019), p. 165268.
[45] N. Narayanan, D. Nk, Materials Research, 21 (2018).
[46] A.K. De, S. Majumdar, S. Pal, S. Kumar, I. Sinha, Journal of Alloys and Compounds, 832 (2020), p. 154127.
[47] L. Singh, M. Hussain, Chalcogenide Lett, 17 (2020), pp. 583-591.
[48] S. Saha, M. Jana, P. Khanra, P. Samanta, H. Koo, N.C. Murmu, T. Kuila, ACS applied materials & interfaces, 7 (2015), pp. 14211-14222.
[49] J. Song, H. Qin, S. Qin, M. Liu, S. Zhang, J. Chen, Y. Zhang, S. Wang, Q. Li, L. Dong, C. Xiong, Materials Horizons, 10 (2023), pp. 2139-2148.
[50] L. Hou, C. Li, X. Wang, X. Wang, T. Wang, Y. Huan, Journal of Advanced Dielectrics, 13 (2022), p. 2242001.
[51] H. Qi, A. Xie, A. Tian, R. Zuo, Advanced Energy Materials, 10 (2020), p. 1903338.
[52] H. Liu, Y.-F. Liu, P.-P. Xiong, P. Chen, H.-Y. Li, J.-W. Hou, B.-N. Kang, Y. Duan, IEEE Transactions on Nanotechnology, PP (2017), pp. 1-1.
[53] A. Sahai, N. Goswami, Structural and optical investigations of oxygen defects in zinc oxide nanoparticles, AIP Publishing.
[54] N. Kandhasamy, G. Ramalingam, G. Murugadoss, M.R. Kumar, G. Manibalan, R. JothiRamalingam, H.M. Yadav, Journal of Alloys and Compounds, 888 (2021), p. 161489.
[55] J.J. William, I.M. Babu, G. Muralidharan, Materials Letters, 238 (2019), pp. 35-37.
[56] A. Laheäär, P. Przygocki, Q. Abbas, F. Béguin, Electrochemistry Communications, 60 (2015), pp. 21-25.

[57] J.J. William, S. Balakrishnan, M. Murugesan, M. Gopalan, A.J. Britten, M. Mkandawire, Materials Advances, 3 (2022), pp. 8288-8297.
[58] R. Mokaya, ION EXCHANGE | Novel Layered Materials: Non-Phosphates, in: I.D. Wilson (Ed.) Encyclopedia of Separation Science, Academic Press, Oxford, 2000, pp. 1610-1617.
[59] Y. Liu, S.P. Jiang, Z. Shao, Materials Today Advances, 7 (2020), p. 100072.
[60] J.J. William, I.M. Babu, G. Muralidharan, Chemical Engineering Journal, 422 (2021), p. 130058.
[61] J.J. William, I.M. Babu, G. Muralidharan, New Journal of Chemistry, 43 (2019), pp. 15375-15388.
[62] J.J. William, I.M. Babu, G. Muralidharan, Surfaces and Interfaces, 42 (2023), p. 103361.
[63] M.A. Raza, Z.U. Rehman, M.G. Tanvir, M.F. Maqsood, 7 - Metal oxide-conducting polymer-based composite electrodes for energy storage applications, in: S. Haider, A. Haider (Eds.) Renewable Polymers and Polymer-Metal Oxide Composites, Elsevier2022, pp. 195-251.
[64] N. Shafiei, M. Nasrollahzadeh, G. Hegde, Chapter 10 - Biopolymer-based (nano)materials for supercapacitor applications, in: M. Nasrollahzadeh (Ed.) Biopolymer-Based Metal Nanoparticle Chemistry for Sustainable Applications, Elsevier2021, pp. 609-671.
[65] M. Li, F. Liu, J.P. Cheng, J. Ying, X.B. Zhang, Journal of Alloys and Compounds, 635 (2015), pp. 225-232.
[66] L. Zhang, K.N. Hui, K. San Hui, H. Lee, Journal of Power Sources, 318 (2016), pp. 76-85.

Statements & Declarations

Funding:

The authors declare that no funds, grants, or other support were received during the preparation of this manuscript.

Ethics declarations

Conflict of Interest

The authors have no relevant financial or non-financial interests to disclose.

Authors Contribution:

The synthesis, formal analysis and first draft of structural, optical, morphological has been done by Dr. Deepannita Chakraborty. Dr. Deepannita Chakraborty also helped in analysing and editing the electrochemical studies part. Dr. S. Maruthamuthu provided this expertise in getting the resources for characterization and in reviewing the electrochemical studies part of the manuscript. Dr.Tholkappiyan Ramachandranhelped in improving the English language and reviewed the whole manuscript giving fruitful inputs for improving the manuscript. The methodology to synthesize is done by Dr.N.Priyadharsin, Dr.S.Kaleemulla helped in obtaining the physical characterization facility for the samples and gave his inputs by reviewing the manuscript.